Nanoscience and Nanotechnology 2016, 6(1A): 18-24
DOI: 10.5923/c.nn.201601.03

Ionic Substituted Hydroxyapatite Scaffolds Prepared by Sponge Replication Technique for Bone Regeneration

Uma Batra[1,*], Seema Kapoor[2]

[1]Department of Materials & Metallurgical Engineering, PEC University of Technology, Chandigarh, India
[2]Dr. S.S. Bhatnagar University Institute of Chemical Engineering & Technology, Panjab University, Chandigarh, India

Abstract Porous metallic implants used for replacement in fractures have well-documented fixation problems, and like natural bone, cannot self-repair or adapt to changing physiological conditions. As a consequence, the implant becomes loose over time. Bioactive ceramic alternatives have shown excellent potential in repair and regeneration of bone defects due to their ability to support bone cell growth and form strong bonds to both hard and soft tissues. This work deals with synthesis and characterization of biodegradable scaffolds with nano-hydroxyapatite (HA), zinc substituted nano-hydroxyapatite (ZnHA) and fluorine substituted nano-hydroxyapatite (FHA) particles for bone regeneration. The nanoparticles were synthesized via wet chemical method and scaffolds were fabricated using sponge replication technique. The elemental composition of nanoparticles was determined using XRF. The crystallography and functional groups were evaluated by XRD and FTIR spectroscopy, respectively. TEM images exhibited the as-synthesized nanoparticles size below 50nm. Zinc/fluorine substitution could affect the ratio of HA and β-TCP (β-tricalcium phosphate) phases in scaffolds. SEM images showed the presence of both macroporosity and microporosity in the scaffolds, with total porosity in the range of 65-75%. From the in-vitro study, it was confirmed that the obtained scaffolds were biomimetic, bioactive, and osteoconductive. Other than bone regeneration, the obtained scaffolds can have a wide array of applications, including tissue engineering, filtration, and catalyst support. The use of ionic substituted hydroxyapatite also opens new possibilities in the field of bone regeneration, utilizing the easily tailored bioactivity and biodegradation rates.

Keywords Hydroxyapatite, Tricalcium phosphate, Scaffolds, Bioactivity, Bone regeneration, In-Vitro

1. Introduction

The bone tissue engineering has focused on the use of natural or synthetic materials in the form of scaffolds as conduits to guide new bone growth in vivo (in the body). The success of tissue engineering is highly dependent upon the properties of the scaffold materials. As such there are four desired characteristics for an ideal material used for making scaffold including osteointegration, osteoconduction, osteoinduction, and osteogenesis [1]. The first three characteristics can be achieved in both biological and synthetic materials, but it is the fourth characteristic that is currently only satisfied by apatitic scaffolds. Pore size, pore structure, surface topography, chemical composition and surface energy are other considerations [2]. The success of scaffolds in-vivo relies on their ability to induce surrounding tissue to invade, grow, and replace the implanted material [3]. In this context, various scaffolds such as HA, tricalcium phosphate (TCP), collagen, chitosan, polycaprolactone (PCL), and poly (lactic-co-glycolic acid) (PLGA), have been used [4], [5].

Biphasic calcium phosphate consists of a bioactive mixture of HA and β-TCP. An optimum balance of the more stable phase of HA and the more soluble β-TCP in scaffold material helps in gradual dissolution in the body, inducing bone regeneration at the expense of biphasic mixture. Moreover, such materials closely resemble natural bone; therefore, foreign body reactions are avoided and bone cells recognize the material. They can also be produced artificially with relative ease and their composition can be varied to alter the degree of biodegradability or to more accurately mirror the chemical composition of bone mineral. Zinc substitution, for example, has shown significant increase in bioactivity in-vitro and improved bone regeneration both in-vivo and clinically. Porous structures have been shown clinically to allow bone in-growth and to provide genuine solutions for the repair of bone defects.

Various modifications such as substitution of desirable ions in apatite, addition of bioactive molecules or nanoparticles can enhance attachment and proliferation of stem cells on the scaffold [6-8]. These scaffolds are more bioactive and responsive to changes in their surrounding

* Corresponding author:
umabatra2@yahoo.com (Uma Batra)
Published online at http://journal.sapub.org/nn

environment [9]. Biological apatites attract special interest for the development of scaffolds because of the proven fact that bioactivity of pure HA is inferior to biological apatite. Thus, the substitutions at the Ca^{2+}, PO_4^{3-} and OH^- sites of HA with several trace elements such as Na^+ (1.0 wt.%), Zn^{2+} (39 ppm), Mg^{2+} (0.60 wt.%), Cl^- (0.10 wt.%), and F^- (0.10 wt.%) may hold the key to improve the biological performance, without altering the basic crystallographic characteristics of HA [10], [11]. Fluorine substitution improves the stability of HA, thus helps in controlling its dissolution rate in physiological environment. Zinc substituted HA nanoparticles containing 1.6 wt.% Zn have been found to enhance bioactivity to human adipose-derived mesenchymal stem cells and antimicrobial capability [12]. Another research also suggests that Zn substituted HA nanoparticles have antibacterial activity and are non-toxic to osteoprogenitor cells [13].

In the present work, an attempt has been made to create scaffolds from zinc substituted and F substituted HA nanoparticles which will possess a good combination of physico-chemical properties, bioactivity and biodegradation.

2. Experimental Procedure

2.1. Synthesis of HA, ZnHA and FHA Nanopowders

HA nanoparticles were synthesized by sol-gel route using calcium nitrate tetrahydrate (CNT, Merck, Germany) and potassium dihydrogen phosphate (KDP, Merck, Germany). 1.0 M solution of CNT and 0.6 M solution of KDP in deionised water was taken in such amounts that Ca/P molar ratio was maintained at 1.67. CNT was added drop by drop gradually to KDP under vigorous stirring using mechanical stirrer (2500 rpm) for one hour. The pH of the solution was maintained at 10 with addition of ammonia solution. In case of ZnHA nanoparticles, 2% zinc nitrate tetrahydrate (ZNT) was added to CNT. (Ca+Zn)/P molar ratio was maintained at 1.67. In case of FHA, a stoichiometric amount of ammonium fluoride (NH4F, Merck, India) was mixed with KDP solution to maintain P/F ratio at 6 to obtain $Ca_{10}(PO_4)_6OH_{2-x}F_x$ for x=1. Gels were obtained and were aged at room temperature for 24 hours. Gelatinous precipitates formed were filtered by a centrifuge and washed thoroughly by double distilled water. The precipitates were dried in an oven at 70°C for 24 hours and the powders were prepared by crushing them with a mortar and pestle. All powders were calcined at 900°C.

2.2. Preparation of HA, ZnHA and FHA Scaffolds

For the synthesis of scaffolds, sponge replication method was used, where polymer sponge of 40 ppi, was cut into pieces of about 10x10x10 mm^3. For the preparation of ceramic slip, the calcined powders were mixed with water containing polyvinyl alcohol, and the latter was varied from 3-10 wt%. The coating was performed by immersing the sponge pieces in the slurry, squeezing them to expel the excess slip. The calcined nanoparticle content was 50 wt. %. The green body was dried for 24 hours at 80°C and heated at a rate of 3°C/min to 800°C for 3 hours, and then further heating at a rate of 3°C/min to the final temperature i.e. 1250°C, where was held for 3 hours to achieve sintering of the mass.

2.3. Characterization of Scaffolds

The morphology and size of nanopowders were observed using Transmission Electron Microscope (TEM, Hitachi, 7500) with resolution of 0.2 nm, operated at an accelerating voltage of 80-100 KV. The powders were ultrasonically dispersed in ethanol to form a dilute suspension and then a drop of suspension was dropped on carbon coated copper grid of 300 mesh for observation. The elemental composition of nanoparticles was determined using wavelength dispersive X-ray Fluoresence Spectroscopy (XRF, Make Bruker, Germany).

The porosity was evaluated using the Archimedes method. The BET surface area of scaffolds was evaluated by N_2 adsorption using Quantachrome Instruments NOVA 2200e Surface Area Analyser using Brunauer–Emmett–Teller (BET) method [14]. The linearized form of BET equation is expressed by:

$$\frac{p}{v(p_o - p)} = \frac{1}{v_m z} + \frac{z-1}{v_m z}\frac{p}{p_o} \quad (1)$$

where p/p_0 is the relative vapour pressure of the adsorbate, v is the volume of gas adsorbed, v_m is the volume of gas adsorbed in a monolayer, and z is a constant related to the energy of adsorption. The minimum relative pressure p/p_0 resolution was 2 x 10^{-5}. A linear regression of the left side of BET equation and p/p_0 yields a slope and intercept from which z and v_m are obtained. The BET surface area is then calculated from v_m.

Infrared spectra (Fourier transform infrared spectroscopy, FTIR Perkin Elmer) were recorded in the region 500–4000 cm^{-1} using KBr pellets (1% wt/wt), with spectral resolution of 2 cm^{-1}, taking four scans for each sample.

X-ray diffraction (XRD, Philips X'Pert 1710) analysis was performed for all powders using Cu K_α radiation, λ = 1.54 Å, 2θ- 20° to 80°, step size 0.017°, time per step 20.03 s, and scan speed 0.005°/s. Relative amount of different phases present in nanoparticles were estimated on the basis of the peak intensity variation by means of external standard method. Crystallinity degree X_c of nanopowders was evaluated as follows:

$$X_c = 1 - V_{112/300} / I_{300} \quad (2)$$

where I_{300} is the intensity of (3 0 0) peak of HA and $V_{112/300}$ is the intensity of the hollow between (1 1 2) and (3 0 0) peaks, which completely disappears in non-crystallline samples. Both cell parameters, a and c were calculated using the equation given below [15]:

$$\frac{1}{d^2} = 4/3 \left[\frac{h^2 + hk + k^2}{a^2} \right] + \frac{l^2}{c^2} \quad (3)$$

where, d is the distance between adjacent planes in the set of Miller indices (h k l), the reference for HA being JCPDS file no. 09-0432 (a = 9.418 Å, b = 9.418 Å, c = 6.884 Å, space group p63/m) and for β-tricalcium phosphate (β-TCP) being JCPDS file no. 09-0169 a = 10.432 Å, b = 10.432 Å, c = 37.39 Å, space group R3c (167)). Crystallite size, X_s of nanoparticle was calculated using Scherrer's equation:

$$X_s = \frac{0.9\lambda}{\beta \cos\theta} \quad (4)$$

where X_S is the crystallite size in nm, λ is the wave length of X-ray beam, β is the broadening of diffraction line at half of its maximum intensity in radians, and θ is the Bragg's diffraction angle (o). The silicon standard was used to measure the instrument broadening in order to correct the value of β. The three diffraction peaks (0 0 2), (2 0 2) and (2 2 2), which are well separated and have high intensities were chosen to calculate mean crystallite size of hydroxyapatite lattice.

The in-vitro behavior of the nanopowders was studied by immersing the nanopowders in simulated body fluid (SBF or Kokubo solution) stored in polystyrene bottles and placed in a biological incubator at 37°C for 12 days. SBF was prepared in double deionized distilled water using various reagents as described earlier [16]. The pH of the solution was measured at an interval of 16 hours using digital pH meter.

The morphological analysis were performed on the obtained scaffolds before and after immersion in SBF by using a Scanning Electron Microscope (SEM, Zeiss) at 20 KV. For SEM analysis, the materials were deposited on side of a double adhesive tape and then stuck to an aluminum stub.

Biodegradation study was carried out by soaking scaffolds in Tris-HCl solution. The solution was kept at 37°C for 7 days and the change in pH of solution and weight loss of the scaffolds were measured.

3. Results and Discussion

In Figure 1, TEM micrographs show that HA and ZnHA had flake-like morphology with an average particle size of 34 ± 6 nm and 21 ± 3 nm, respectively; whereas, FHA nanoparticles consisted of rod-like particles having average length as 29 ± 7 nm, and diameter as 4.2± 0.4 nm, respectively. Due to F- incorporation in HA lattice, the morphology changed from flake-like to rod-like.

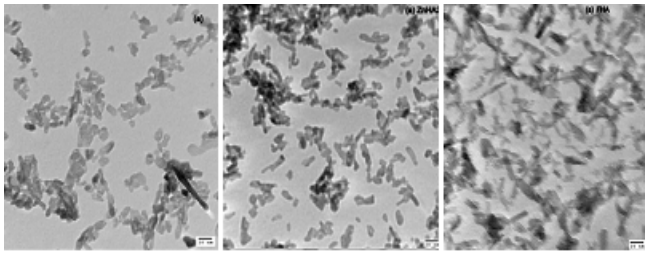

Figure 1. TEM images of HA, ZnHA, and FHA nanoparticles

The Ca/P ratio was 1.67 and zinc content in ZnHA was 3.9 mol% (by XRF analysis). Figure 2 presents the scaffolds prepared for investigation. The resultant scaffolds after sintering at the 1250°C, were strong enough to sustain careful handling.

Figure 2. HA-S, ZnHA-S, and FHA-S scaffolds prepared in present work

Figure 3 shows the SEM images of scaffolds. The scaffolds exhibited macroporosity (100-200µm) as well as the microporosity (1-10µm). The interconnectivity and good sintering features are clearly visible. Thus, sponge replication technique resulted in highly porous scaffolds with suitable pore size and morphology for cell colonization. This macroporosity is one of the mandatory characteristics for any bone substitute, if it is to be effective in terms of cellular adhesion and proliferation into concavities acting as protective niche for osteogenic cells. On the other hand, scaffolds that have a predominantly convex surface, such as rounded or tubular, do not provide bone cells with a favourable environment. The minimum pore diameter required for bone in-growth and angiogenesis into a scaffold is considered to be at least 100µm [17]. Previous in-vitro studies have suggested that the ideal pore diameter for bone in-growth is between 300 and 400µm [18], [19]. Here, macropores with 100-200µm with concavity make the scaffold osteoconductive. The porosity was inversely related to PVA concentration. The porosity of 75, 72, 70, 67 and 65% was obtained for 3, 5, 6, 7.5, and 10 wt.% PVA concentration in slurry, respectively. However, the porosity did not alter with zinc or fluorine substitution in nanoparticles.

The presence of micropores, 0.1–5µm in size, ascribable to solvent extraction by solvent evaporation, may concur to enhance the surface area for cell attachment and protein adsorption [20]. The microporosity is crucial for enhancing the bioactivity of scaffolds by allowing for penetration of biological fluids. The higher is the microporosity, the higher will be the BET surface area (SSA) which enhances protein adsorption and osteoinductive trophic factor. The BET surface area for HA-S, ZnHA-S, and FHA-S scaffolds was 6, 8, and 10 m^2/g respectively. The typical BET surface area of a non-microporous scaffold is below 1 m^2/g. Thus, the present scaffolds can be both osteoconductive and bioactive.

The Ca/P molar ratio (by XRF and EDS analyses) was 1.67, 1.58, and 1.66 for HA-S, ZnHA-S, and FHA-S, respectively. The F content was measured as 2.18 (±0.02) wt.% for FHA-S representing substitution levels of 58 % (the F content of stoichiometric FA is 3.77 wt.%). The measured density of samples sintered at 1250°C was 28 ± 1% of the

theoretical density (TD = 3.156 g.cm^{-3}) corresponding to a porosity fraction of about 72 ± 1%.

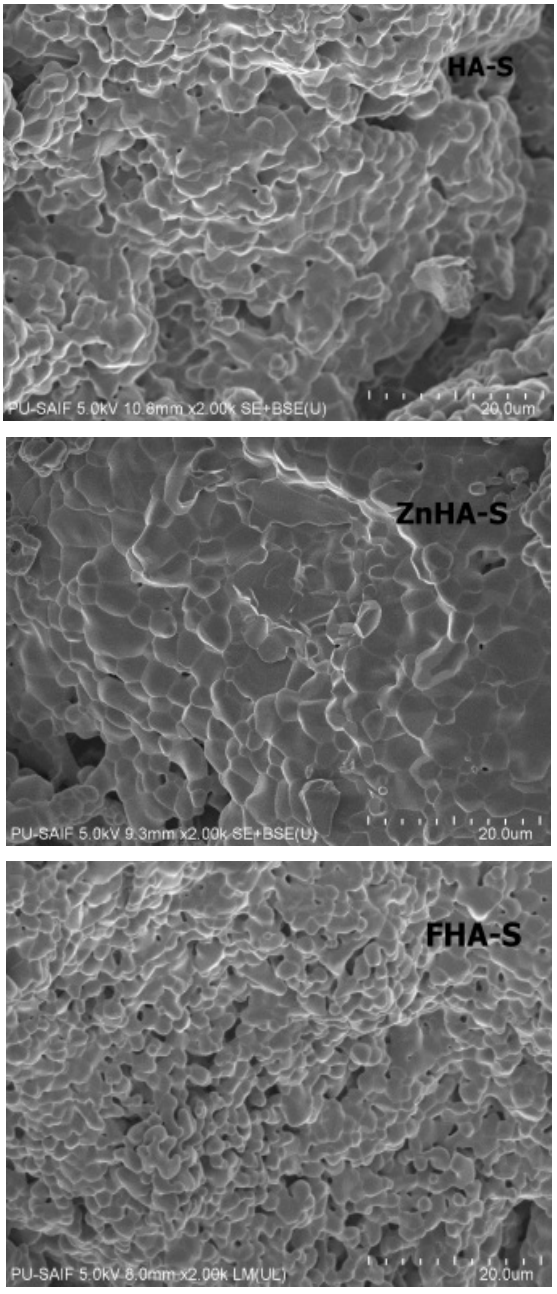

Figure 3. SEM images of HA-S, ZnHA-S, and FHA-S scaffolds

The FTIR spectra of HA, ZnHA-S and FHA-S (Figure 4) show all characteristic absorption peaks of stoichiometric pure hydroxyapatite. The first indication of the hydroxyapatite formation is in the form of broad FTIR band centered at about 1000–1100 cm^{-1}. The bands at 960–965 cm^{-1} and at 565–601 cm^{-1} correspond to ν_1 and ν_4 symmetric P–O stretching vibration of the PO_4^{-3} ion, respectively [23]. As a major peak of phosphate group, the ν_3 vibration peak could be identified in the region between 1100 cm^{-1} and 960 cm^{-1}, which is the most intensified peak among the phosphate vibration modes. The band between 565 cm^{-1} and 601 cm^{-1} belongs to ν_4 vibration mode of phosphate group which occupies two sites in the crystal lattice (at 601 cm^{-1} and 567 cm^{-1}). The presence of weak bands of the CO_3^{2-} group (1415, 1450 and very weak 1540 cm^{-1}) indicate that it is slightly carbonated hydroxyapatite. The presence of carbonates in apatite lattice (Figure 4) is an important feature for the biological performance of apatites as implants. The peak at 1040 cm^{-1} is the triply degenerated vibration, ν_3, while 946 cm^{-1} is the non-degenerated symmetric stretching mode, ν_1, of P–O bond of the phosphate group. The peaks at 603 and 565 cm^{-1} are assigned to bending mode, ν_4, of the O–P–O bond. Thus, the formation of HA was confirmed by FTIR spectra due to the presence of the stretching and bending modes of PO_4^{-3}. The bands assigned to the stretching modes of hydroxyl groups (OH^-) in the hydroxyapatite at 3660 cm^{-1} can be clearly observed in the spectra. The broad envelope at about 3400 cm^{-1} was due to the O–H stretching of water, typical of HA. The intensity of this peak was similar in HA-S and FHA-S, but it was lesser in ZnHA-S, suggesting the development of β-TCP phase.

The XRD patterns (Figure 5) of HA-S, ZnHA-S and FHA-S scaffolds show that HA-S consisted of pure hydroxyapatite phase, whereas, ZnHA-S and FHA-S consisted of biphasic mixture of HA and β-TCP. The formation of higher amount of β-TCP in case of ZnHA-S (Table 1) can be considered advantageous, since the biphasic scaffold materials produced can combine bioresorbable β-TCP and stable HA. The comparison of the patterns of standard FA (00-71-0880) and HA (00-009-0432) to each particular peak of the XRD pattern of Figure 5 reveals that the peaks of HA and ZnHA fitted to the pattern of stoichiometric HA, whereas peaks of FHA fitted much better to the patterns of FA than to HA. Table 1 presents the crystallinity, crystallite size and lattice parameters 'a' and 'c' of HA-S, ZnHA-S, and FHA-S after sintering at 1250°C.

The fluorine substitution in HA caused increase in the crystallinity (Table 1). The crystal sizes in HA-S, ZnHA-S and FHA-S are also given in Table 1. The peak positions of HA-S did not exhibit a significant difference, in comparison with the pattern for ZnHA-S and FHA-S. The lattice parameters of HA-S, ZnHA-S and FHA-S and standard HA (00-009-0432) and FA (00-071-0880) are also presented in Table 1.

Table 1. Crystallinity, crystallite size and lattice parameters of HA-S, ZnHA-S, and FHA-S sintered at 1250°C

Scaffold	X_c	Xs (nm)	Lattice Parameter		HA:β-TCP	Ca/P
			a, Å	c, Å		
HA-S	0.92	96.8	9.408	6.887	100:00	1.67
ZnHA-S	0.91	72.1	9.405	6.921	51:49	1.58
FHA-S	0.99	110.9	9.374	6.888	87:13	1.66
FA (00-71- 0880)	-	-	9.363	6.878	-	-
HA (00-009-0432)	-	-	9.418	6.884	-	-

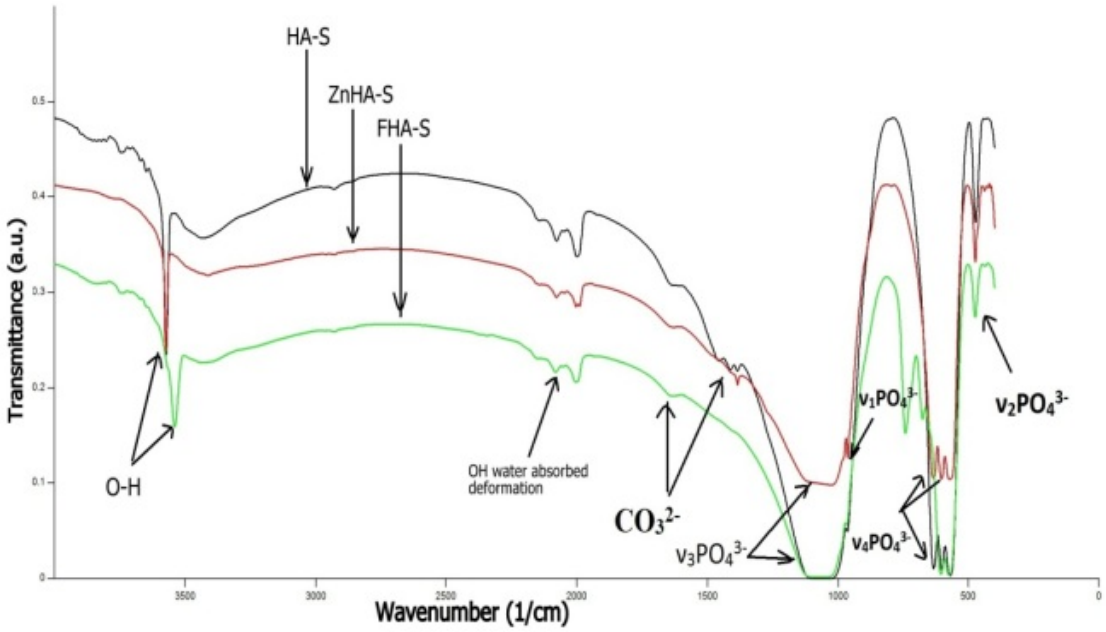

Figure 4. FTIR spectra of HA-S, ZnHA-S, and FHA-S scaffolds

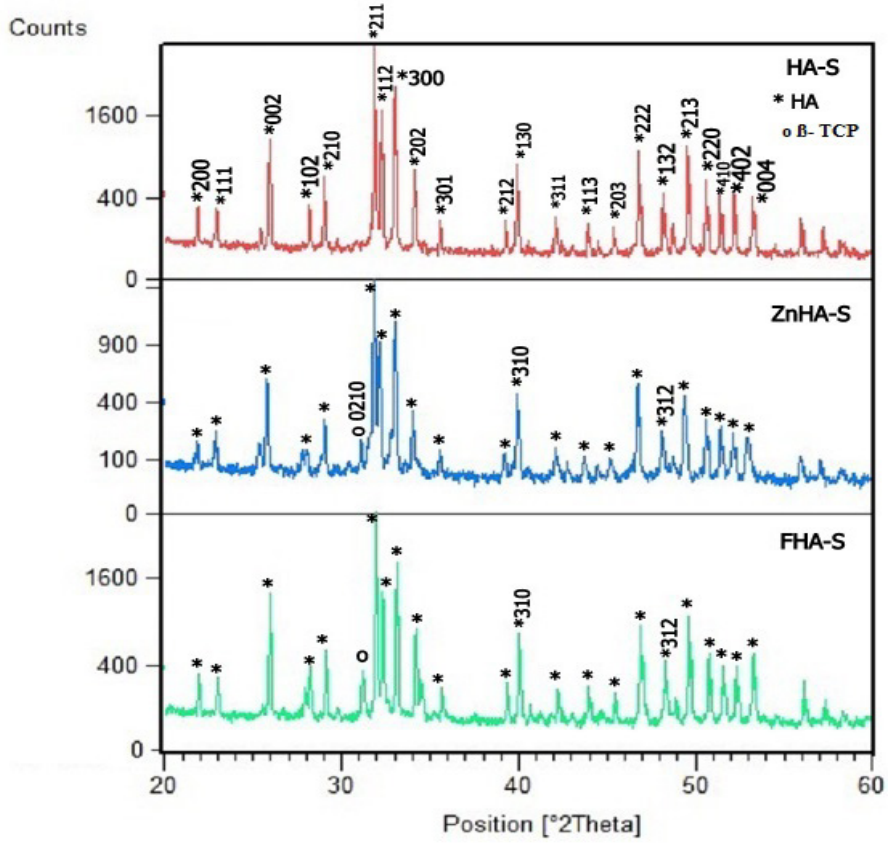

Figure 5. XRD patterns of HA-S, ZnHA-S, and FHA-S scaffolds

Compared to HA, the F fluorine substitution in FHA caused lowering of the a-axis value (Table 1). These results agree fairly well with earlier studies [22]. The SEM images of HA-S, ZnHA-S and FHA-S scaffolds after treatment in SBF solution (IvHA-S, IvZnHA-S and IvFHA-S) are shown in Figure 6. During in-vitro experiments, mineral crystals grew on all scaffolds (Figure 6) after 12 days in physiological solution; nevertheless, IvZnHA-S indicated the most uniform growth.

The mineral that grew on the scaffold surface was confirmed to be hydroxyaptite from FTIR spectra (Figure 7) of dried IvHA-S, IvZnHA-S and IvFHA-S scaffolds. Thus,

the obtained scaffolds were biomimetic and osteoinductive. The starting pH of SBF solution was 7.2, which increased to 7.9 in 48 hours of immersion; when SBF was replaced by a freshly prepared SBF and pH was brought down to 7.4; the pH once again increased to 8.0 after 48 hours. This behaviour was continuously displayed till the time of experiment of 12 days. Thus, it is suggested that the obtained scaffolds are bioactive.

Biodegradation of scaffolds behaviour was studied by immersing the scaffolds in Tris-HCL buffer solution at pH 7.4 maintained at 37°C for 7 days. The pH of buffer increased from 7.4 to 7.8; and there was a 3-5% weight loss of the scaffolds, which suggested that the obtained scaffolds are biodegradable.

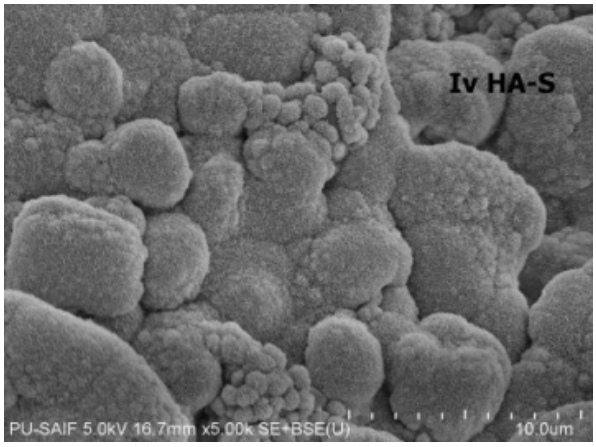

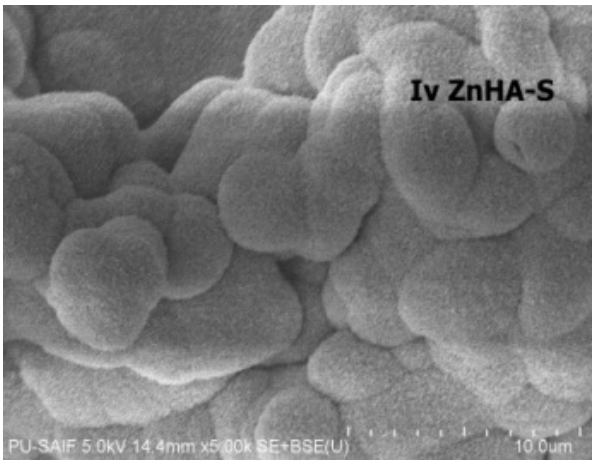

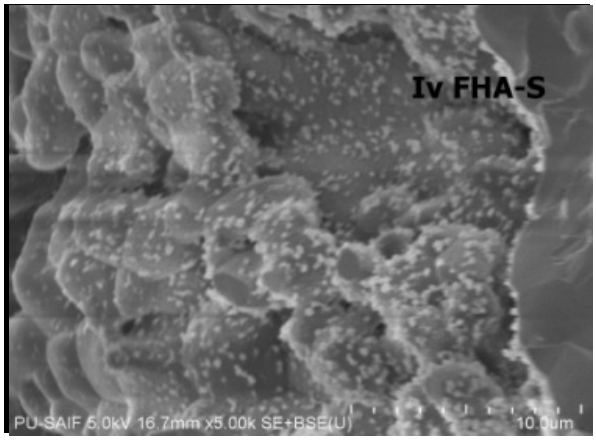

Figure 6. SEM images of HA-S, ZnHA-S, and FHA-S scaffolds after immersion in SBF for 12days

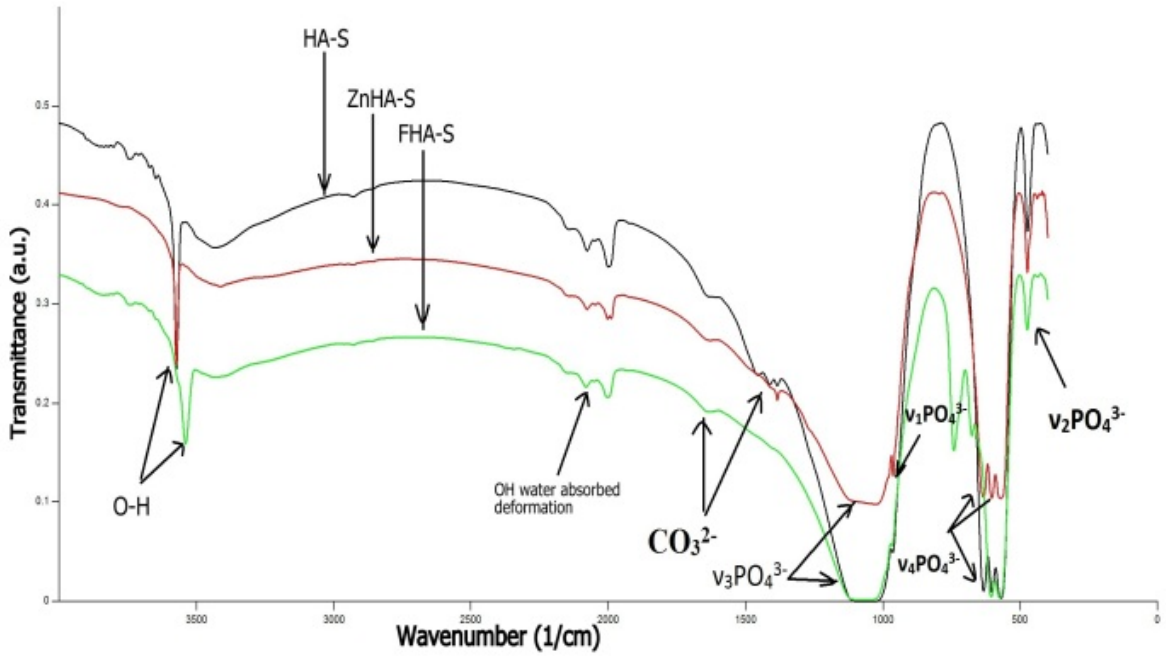

Figure 7. FTIR spectra of HA-S, ZnHA-S, and FHA-S scaffolds after immersion in SBF for 12 days

4. Conclusions

This paper has proposed a new strategy for smart scaffold manufacturing, combining sponge replication technique with ionic substitution in nano-hydroxyapatite particles. The process is easy to carry out and does not require specialized equipments. The scaffolds have porosities of 65-75%. Increase in PVA led to decrease in porosity of the material. The scaffolds had macroporosity in the range of ~100-200μm and the pores were inter-connected. Microporosity was in the range of ~ 1-10μm. An appreciable amount of hydroxyapatite growth on these scaffolds formed when immersed in SBF for 12 days. In case of ZnHA-S apatite, growth was the most uniform. The biphasic mixture of 49% HA and 51% TCP in ZnHA-S appeared to have optimum balance and responsible for controlled resorbability. Thus, it can be concluded that the bone intrusion can possibly be tailored in calcium phosphate based scaffolds by adjustment of amounts of HA (biocompatible phase) and TCP (bioresorbable phase). The obtained scaffolds have the combined features of macroporosity, microporosity, apatite forming ability; therefore can be believed to possess the essential characteristics of a smart scaffold such as biomimicry and osteoinductive/ osteopromotive, bioactivity and osteoconductivity. Thus it can be concluded that the "smart scaffolds" can be created for bone regeneration applications by the proposed integrated approach.

REFERENCES

[1] M.B. Nair, S. Suresh Babu, H. K. Varma, and A. John, A triphasic ceramic-coated porous hydroxyapatite for tissue engineering application, Acta Biomaterialia, 4, 173, 2008.

[2] G. M. Crane, S. L. Ishaug, and A. G. Mikos, Bone tissue engineering, Nature Medicine, 1, 1322, 1995.

[3] J. H. Shepherd, S. M. Best, Calcium phosphate scaffolds for bone repair, J of Metals, 63,83–92, 2011.

[4] A. Khojasteh, H. Behnia, S. G. Dashti, M. Stevens, Current trends in mesenchymal stem cell application in bone augmentation: A review of the literature. J Oral Maxillofac Surg., 70, 972–982, 2012.

[5] F. S. Tabatabaei, S. R. Motamedian, F. Gholipour, K. Khosraviani, A. Khojasteh, Craniomaxillofacial bone engineering by scaffolds loaded with stem cells: A Systematic Review, J Den Sch, 30,113–130, 2012.

[6] A. Abarrategi, C. Moreno-Vicente, V. Ramos, I. Aranaz, J. V. Sanz Casado, J. L. López-Lacomba, Improvement of porous beta-TCP scaffolds with rhBMP-2 chitosan carrier film for bone tissue application, Tissue Eng Part A., 14,1305–1319, 2008.

[7] C. Xu, Y. Wang, X. Yu, X. Chen, X. Li, X. Yang, S. Li, X. Zhang, A. P. Xiang, Evaluation of human mesenchymal stem cells response to biomimetic bioglass-collagen-hyaluronic acid-phosphatidylserine composite scaffolds for bone tissue engineering, J Biomed Mater Res A, 88, 264–273, 2009.

[8] X. B. Zeng, H. Hu, L. Q. Xie, F. Lan, W. Jiang, Y. Wu, Z. W. Gu, Magnetic responsive hydroxyapatite composite scaffolds construction for bone defect reparation, Int J Nanomedicine, 7, 3365–3378, 2012.

[9] B. D. Ratner, S. J. Bryant, Biomaterials: Where we have been and where we are going, Annual Rev Biomed Eng, 6, 41–75, 2004.

[10] R. Z. Le Geros, J. P. Le Geros, Dense hydroxyapatite. In: Hench LL, Wilson J, editors. Introduction to bioceramics, Singapore: World Scientific, 139, 1993.

[11] S. Cazalbou, C. Combes, D. Eichert, C. Rey, Adaptative physicochemistry of bio-related calcium phosphates, J Mater Chem,14, 2148–53, 2004.

[12] Thian, E.S., Konishi, T., Kawanobe, Y., Lim, P.N., Choong, C., Ho, B., Aizawa, M., Zinc-substituted hydroxyapatite: a biomaterial with enhanced bioactivity and antibacterial properties, J Mater Sci Mater. Med,24,437–445, 2013.

[13] M. Swetha, K. Sahithi, A. Moorthi, N. Saranya, S. Saravanan, K. Ramasamy, N. Srinivasan, N. Selvamurugan, Synthesis, characterization, and antimicrobial activity of nano-hydroxyapatite-zinc for bone tissue engineering applications. J., NanosciNanotechnol, 12, 167–172, 2012.

[14] R. Joseph, K. E. Tanner, Effect of morphological features and surface area of hydroxyapatite on the fatigue behavior of hydroxyapatite-polyethylene composites, Biomacromol, 6,1021–1026, 2005.

[15] T. J. Webster, E. A. Massa-Schlueter, J. L. Smith, E. B. Slamovich, Osteoblast response to hydroxyapatite doped with divalent and trivalent cations, Biomaterials, 25, 2111–2121, 2004.

[16] T. Kokubo, Formation of bone like apatite on metals and polymers by biomimimetic process, Biomaterials, 12, 155–163, 1996.

[17] G. Daculsi, S. Baroth, R. Le Geros, 20 years of biphasic calcium phosphate bioceramics development and applications, Advances in Bioceramics and porous ceramics II, 45–58, 2010.

[18] E. Tsuruga, H. Tahita, H. Itoh, Y. Wakisaka, Y. Kuboki, Pore size of porous hydroxyapatite as the cell-substratum controls BMP-induced osteogenesis, J Biochem, 121(2),317–24, 1997.

[19] W. J. Li, R. Tuli, X. X. Huang, P. Laquerriere, R. S. Tuan, Multilineage differentiation of human mesenchymal stem cells in a three-dimensional nanofibrous scaffold, Biomaterials, 26(35), 5158–5166, 2005.

[20] P. X. Ma, R. Zhang, G. Xiao, R. Franceschi, Engineering new bone tissue in vitro onhighly porous poly(a-hydroxyl acids)/hydroxyapatite composite scaffolds, J Biomed Mater Res, 54(2), 284–293, 2001.

[21] F. Miyaji, Y. Kono, Y. Suyama, , Formation and structure of zinc–substituted calcium hydroxyapatite, Mater Res Bull, 40, 209–213, 2005.

[22] S. Kannan, J. M. Ventura, J. M. F. Ferreira, In situ formation and characterization of fluorine-substituted biphasic calcium phosphate ceramics of varied F-HAP/β-TCP ratios, Chem Mater, 17, 3065–3068, 2005.